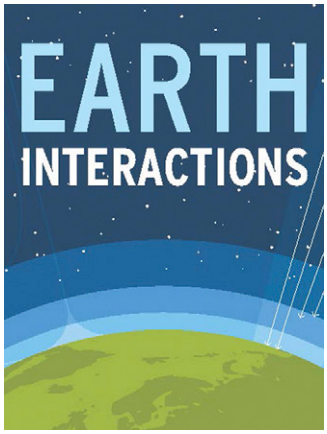

The Centennial Variation of El Niño Impact on Atlantic Tropical Cyclones

Ruixin Yang[a]

Department of Geography and Geoinformation Science, College of Science, and Center for Earth Observing and Space Research, George Mason University, Fairfax, Virginia

Allison Fairley

Department of Geography and Geoinformation Science, College of Science, George Mason University, Fairfax, Virginia

Wonsun Park

GEOMAR Helmholtz Centre for Ocean Research Kiel, Kiel, Germany

Received 4 April 2017; in final form 24 October 2017

ABSTRACT: Predicting tropical cyclone (TC) activity becomes more important every year while the understanding of what factors impact them continues to be complicated. El Niño–Southern Oscillation (ENSO) is one of the primary factors impacting the activities in both the Pacific and the Atlantic, but an extensive examination of the fluctuation in this system has yet to be studied in its entirety. This article analyzes the ENSO impacts on the Atlantic tropical cyclone activity during the assessed warm and cold years to show the dominant centennial-scale variation impact. This study looks to plausibly link this

[a]*Corresponding author*: Ruixin Yang, ryang@gmu.edu

DOI: 10.1175/EI-D-17-0006.1

variation to the Southern Ocean centennial variability, which is rarely mentioned in any factors affecting the Atlantic tropical cyclone activity. This centennial variability could be used to enhance future work related to predicting tropical cyclones.

KEYWORDS: Tropical cyclones; Atmosphere−ocean interaction; Climate variability; El Niño; ENSO; Time series

1. Introduction

Tropical cyclones (TCs) in general, or hurricanes [TCs with wind speed higher than 63 kt (1 kt = 0.51 m s^{-1})] in particular, are of significant interest to the scientific community as well as the general public. Further understanding of what causes TCs to develop, intensify, and change paths will continue to be of interest to the general public as TCs continue to impact a large portion of the world population. In an era of knowledge sharing and accessibility, continuing to develop and aggregate information to make decisions is very important. Shedding light on what could cause shifts in TC patterns (short or long scale) and further enhancing the scientific community's ability to understand the inner workings of the TCs will enable the public to further understand TCs and make better decisions such as locations of vacations and new homes. In addition to the short-time TC forecasting as part of weather forecasting (e.g., real-time tropical weather forecasting at http://www.nhc.noaa.gov/), seasonal forecasting also attracts the attention of the TC researchers. Among most seasonal TC forecasting schemes, the climate variability associated with the so-called El Niño and La Niña phenomena plays an important role.

The indicator of El Niño or La Niña is the central and eastern Pacific sea surface temperature (SST) fluctuation. When the 3-month average SST anomaly (SSTA) over the Niño-3.4 region (5°N–5°S, 120°–170°W) is higher than 0.5°C in five consecutive months, a warm episode, or El Niño, takes place. The opposite cold episode, or La Niña, corresponds to SSTA being less than −0.5°C in the same condition [Climate Prediction Center (CPC) 2015].

Complimentary to these anomalous SST values, extreme fluctuations of atmospheric pressure at sea level are also identified throughout the Pacific Ocean, which is commonly known as the Southern Oscillation. These variations from the norm between the western and eastern Pacific are described by the Southern Oscillation index (SOI). The variation of the Pacific SST and the fluctuation of the pressure difference are highly correlated, and they are together called the El Niño–Southern Oscillation (ENSO). The periods of large negative values of SOI correspond to warm episodes in the eastern Pacific (Philander 1990; Hanley et al. 2003).

Although ENSO is a phenomenon in the tropical Pacific, its impacts reach many regions far from the Pacific. One commonly accepted and widely mentioned impact is that El Niño suppresses and La Niña enhances the TC activities (seasonal hurricane days and hurricane numbers) in the Atlantic basin (Gray 1984; Stevenson 2012; Patricola et al. 2015). The major mechanism for the ENSO role in the Atlantic TC activities is that ENSO changes one of the most important factors affecting TC development, the unfavorable vertical wind shear. El Niño leads to increased vertical wind shear in the Atlantic while La Niña decreases the shear (Gray 1984; Patricola et al. 2015).

Because of the important role of ENSO in Atlantic TC activities, most seasonal prediction schemes of the Atlantic TC activities use ENSO components as one of the predictors (Klotzbach 2007, 2011; Davis et al. 2015). Most discussions on the trend changes of TC activities in perspective of climate change is also in the context of ENSO and/or SST changes (Goldenberg et al. 2001; Webster et al. 2005; Emanuel 2005; Mann et al. 2009). Nevertheless, the ENSO impact on the Atlantic TC activities is not uniform for long time periods. For example, Gray (1984) did not find the same relationship between ENSO and Atlantic TC activities for data covering the nineteenth century and attributes that to data quality. Additionally, different ENSO influences on TC activities for below-normal and above-normal periods have been identified, and it was demonstrated that the ENSO impacts can be masked by multidecadal signals (Bell and Chelliah 2006). Other studies modulate the ENSO impact based on the phases of the Atlantic multidecadal oscillation (AMO; Davis et al. 2015).

Since the ENSO impact on the Atlantic TC activities is time dependent, the impact itself may show certain variation. What is the quantitative description of this impact as a function of time? Are there any patterns in the impact variation with time? What causes this pattern? Here, we evaluate the historical ENSO data and its impact on the Atlantic TC activity (defined by number of named storms) in an innovative way to assess how the impact changes over time on a centennial time scale and what possibly causes the variation. The results are potentially helpful for long-term prediction of the Atlantic TC activity beyond seasonal and decadal scales.

2. Datasets and methods

Several datasets are utilized for this study. The data of cold and warm episodes are given by the CPC of the U.S. National Oceanic and Atmospheric Administration (NOAA) from 1950 to present based on the monthly SSTA in the Niño-3.4 region (CPC 2015). Although the CPC definition is the commonly accepted standard for El Niño and La Niña definitions, the covered time period is too short for the intended analysis of long-term ENSO impact on the Atlantic TC activity. To have a longer time series, the commonly used alternative SOI dataset, from NOAA Earth System Research Laboratory (ESRL), is also used. These data cover the period from 1866 to present with monthly temporal resolution (ESRL 2015). The TC activity dataset is the NOAA Atlantic hurricane database (HURDAT) from 1851 to present, which records the number of named storms, hurricanes, major hurricanes, and the accumulated cyclone energy (ACE) for each year [Landsea et al. 2010; Hurricane Research Division (HRD) 2015]. As is widely known, the number of records for earlier years before the availability of the satellite observations is lower than the reality (Landsea and Franklin 2013). However, the main intent of using this data is to compare the difference in similar time periods, and the undercounting will not be an issue for this purpose (Klotzbach 2011). In this study, the cutoff time is December 2014.

The first task for utilizing a long time series is to use SOI data to define the warm and cold episodes that are close to those defined by SSTA. Simply using

threshold values to define warm and cold episodes based on SOI results in a large discrepancy between the SOI-based definition and the definition by SSTA no matter how the threshold values are adjusted. To improve the agreement of the two definitions, we mimic the SSTA treatment by using a 3-month moving average and at least five consecutive-averaged SOI values lower (higher) than the warm (cold) SOI threshold value to define a warm (cold) episode. The SOI values are first filtered with a 3-month moving average. The smoothed data are checked with a warm (cold) threshold value. If there are at least five consecutive-averaged SOI values smaller (larger) than the warm (cold) threshold value, it is concluded that there is a warm (cold) episode. If the August–October (ASO)-averaged SOI is in the warm (cold) episode, the corresponding year is defined as a warm (cold) season.

With the long-term warm and cold episodes defined with SOI values, the numbers of named storms (tropical storms, hurricanes, and subtropical storms; HRD 2015) in HURDAT are counted for warm and cold episodes. Basic statistics including differencing, moving average, correlation, and Fourier analysis are applied to the counted numbers.

3. Results

3.1. Long-term warm and cold episodes defined with SOI

Unlike the fixed SSTA threshold values, ±0.5°C used by CPC (2015) in the warm/cold episode definition, the threshold values mentioned above for SOI are adjusted to search for the best results, the least discrepancy between the SOI-based episodes and the SSTA-based episodes. This research shows that the discrepancy is sensitive for the cold threshold. The best result is obtained when the threshold value is 0.42. That is, if the ASO-averaged SOI is higher than 0.42 within five consecutive such ‘‘high’’ months, that season is defined as the cold season. With this definition, one can find that in the SOI and SSTA overlapping period 1950–2014, there are 3 years being identified as cold years with SOI but not with SSTA. On the other extreme, 4 years are missed, and this gives a total seven mismatches for cold seasons. On the contrary, the impact of the warm threshold values is much more stable. With all values between −0.54 and −0.39, the outcomes are the same. When the threshold value is set to be −0.39, there are two extra warm seasons and three missed seasons with a total of five mismatches. When the threshold values change between −0.54 and −0.39, the specific mismatched years may be different but the total number of mismatches remains at 5.

Figure 1 displays the time series of ASO SOI values and the warm (cold) seasons defined above with −0.39 (0.42) as the warm (cold) threshold value. One can see that there are roughly seven warm seasons in 20 years, consistent with the 2–7-yr period of the ENSO phenomenon. From this figure, one can easily identify the misses or ‘‘false hits’’ when compared to the SSTA-based warm or cold seasons after the 1950 season. For example, the two open circles represent the two seasons, 1992 and 1993, which are identified as warm seasons by SOI but not by SSTA. These are the false hits. On the other hand, the three crosses without circles, representing 1968, 1976, and 1986, denote warm seasons identified by SSTA but failed to be selected by SOI. These are the misses. All other warm seasons are

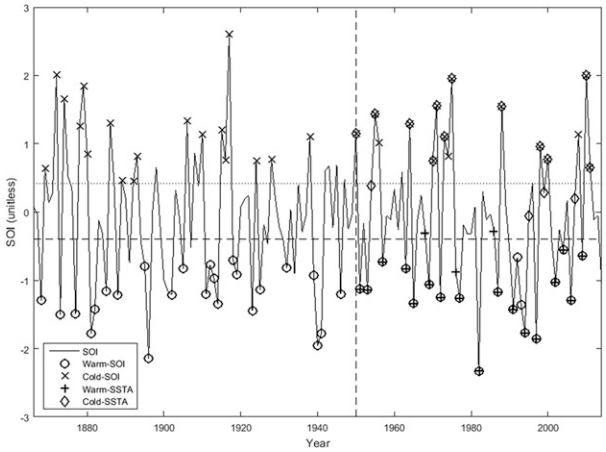

Figure 1. SOI values with warm and cold seasons. The SOI values displayed are the 3-month moving average value at September (ASO) for each year. The vertical dashed line is the start year (1950) with Niño-3.4 SSTA defined warm and cold episodes. The dashed horizontal is the maximum threshold values (−0.39) for defining the SOI-based warm episodes, and the dotted horizontal line is the minimum value (0.42) for defining the cold episode.

detected by both SOI and SSTA. The detection of cold seasons has a relatively large difference with four misses (open diamonds for 1954, 1995, 1999, and 2007) and three false hits (unenclosed X symbols for 1956, 1974, and 2008).

3.2. Variation of the ENSO impacts

With warm and cold episodes defined based on SOI values, long-term counts of named storms for each category of the episodes become possible. Here, a 31-yr moving average is used to smooth the results. That is, 31 years are selected to be the time period, and the mean counts of named storms in all warm seasons and all cold seasons during the selected 31 years are calculated.

Figure 2 gives the 31-yr moving average counts of named storms in the Atlantic in warm and cold seasons. For example, in the 31-yr period 1866–96, denoted by the midyear 1881, the average number of named storms is 6.7 in warm years and 9.8 in cold years. Since the 1-yr shift of the 31-yr window may not result in any changes in the members of warm and cold groups, there are many short flat segments in the counts of the named storms. This figure clearly demonstrates the commonly accepted relationship between ENSO and TC activity in the Atlantic, cold episodes being favorable to TCs and warm episodes depressing TCs as the cold average is always higher than the warm average. However, this relationship is only significant for certain periods such as the most recent period starting in the 1980s. In the middle part of the whole study time range, from the early 1920s to late 1970s, although the difference is evident with cold counts being larger than the warm counts, it is difficult to say the difference is substantial. To quantify the differences, the one-tail *t* test for two means assuming unequal variances is carried

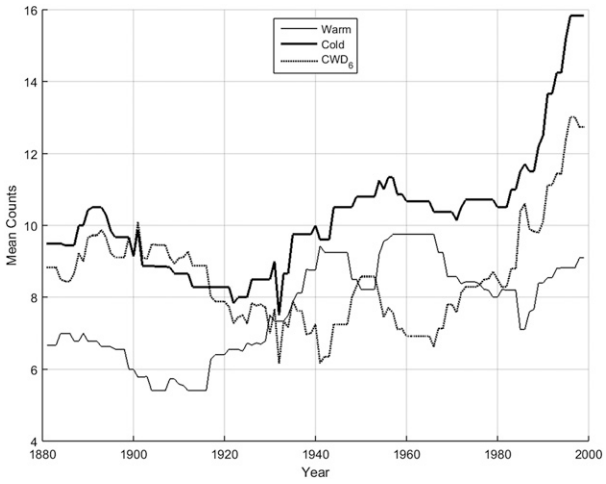

Figure 2. Average counts of named storms in warm and cold seasons and their differences with a 31-yr moving window. The year in abscissa is the middle year of the 31-yr period. The cold/warm difference is shifted by 6 (with CWD_6 = cold number − warm number + 6) for display purpose.

out for each period. As expected, the difference is significant at a 0.05 significance level before 1902 and after 1984 only. In between, the p values (not shown) are larger than 0.05. If the significance is set at 0.1, the middle insignificant period will be reduced from 1902 to 1984 to 1908 to 1982 with two subperiods, 1950–53 and 1978–80, as exceptions.

In addition to the warm and cold mean counts in Figure 2, the difference between the cold means and the warm means [cold warm difference (CWD)] is also displayed. This shows that the difference changes in a very low frequency, and along the large-scale variation, there are relative high-frequency but small-amplitude oscillations. The entire dataset seems to cover only one oscillation period, from 1881 to 1999, giving an oscillation with the longest period of 118 years. When longer time series of TC activity are available, this variation should be revisited carefully. Figure 3 shows spectral power based on Fourier analysis of the CWD values and confirms the observation. The Fourier components are converted into percentage of the total power in the plot. The dominant component with the 118-yr period has 58.8% of all power, and the component with the second (third) highest power is the one with the 39.3-yr (19.7 yr) period and 11.9% (6.40%) of the power. There are only five other components with larger than 1% of the total power but all less than 4%.

3.3. Driving factor(s)

What causes the low-frequency changes of ENSO impact to the Atlantic TC activity? First, we turned to well-known existing climate indices. Many climate indices are created to represent various types of climate variability. For example, ESRL listed many such indices from popular SOI and North Atlantic Oscillation

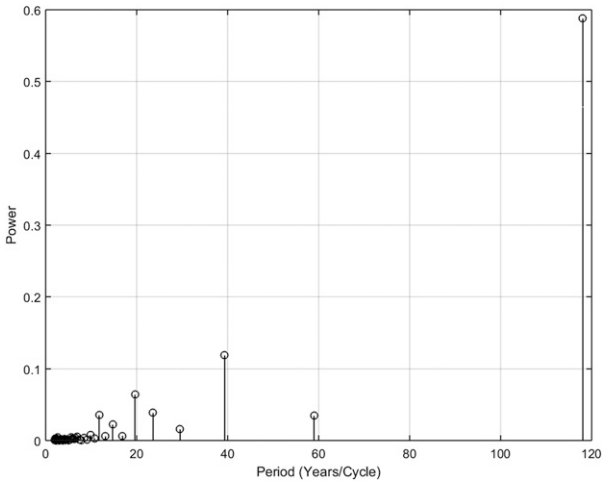

Figure 3. Spectral power of CWD. The power values displayed are normalized to make the total power be one.

(NAO) to regional specific northeast Brazil rainfall anomaly to even solar flux (ESRL 2017). Many natural phenomena and their changes including TC activities are correlated to those climate indices (Goldenberg et al. 2001; Cobb et al. 2013). Most of these indices demonstrate variability in seasonal to interannual or decadal scales. Commonly mentioned climate indices with low frequency from decadal to centennial scales include AMO (Enfield et al. 2001), NAO (Hurrell 1995; Jones et al. 1997), Pacific decadal oscillation (PDO; Zhang et al. 1997), and the tripole index for the interdecadal Pacific oscillation (TPI; Henley et al. 2015), and those indices are related to the Atlantic TC activity. For example, Biondi et al. (2001) used tree-ring data to investigate the PDO variability and identified a bidecadal mode. Interestingly, the dominant negative phase identified by their first principal component (1945–70 in their Figure 3) is partially coincident with the lowest TC count difference between the warm and cold episodes (1918–71 by using 2 as the threshold for the count difference except for a subperiod 1948–54), but the overall trends in the nearby periods are quite different. Moreover, no single index, among those commonly studied, actually shows variability with such a low frequency for a period longer than a century.

Climate indicators with a longer time scale also exist. Minobe (1997) investigated instrumental spring air temperature in western North America, winter–spring sea level pressure (SLP) in the central North Pacific and SST in various regions and found climate regime shifts in the 1940s and 1970s. Earlier shifts also appear in some but not all of the data. Using the multitaper method (MTM), Minobe (1997) found the periods of those time series are between 50 to 70 years. Furthermore, Minobe (1997) used the tree-ring-based constructed data in North America to confirm the findings in regime shifts and the 50–70 oscillation periods with the first EOF mode.

The climate index with the lowest frequency other than those on proxy data of paleoclimate scales in literature is possibly the Southern Ocean centennial

variability (SOCV) index identified by Latif et al. (2013). SOCV, representing the centennial-scale internal variability in the Southern Ocean, is based on the Southern Ocean SST anomaly averaged over the latitude band 50°–70°S. Latif et al. (2013) attribute the centennial variability to deep-ocean convection and link Arctic and Antarctic sea ice extent phase discrepancy, recent slowing of mean global air temperature increase, and even the change of the southern annular mode (SAM) to SOCV. The SOCV shows a 100-yr period (Figure 2a in Latif et al. 2013), although the simulation results and tree-ring-based proxy data indicate a period ranging from 200 to 500 years.

Because of the similar periodicities between SOCV and the TC count difference in warm and cold eastern Pacific episodes, it is hypothesized that the two phenomena are correlated to each other. To quantify the relationship, correlation analysis is conducted between the count difference and SOCV as well as other climate indices mentioned above. SOI is also included in the correlation analysis, although it actually shows mainly seasonal to interannual variability. Initially, Pearson's r correlation was employed. However, the Shapiro–Wilks test results show that the CWD values do not follow a normal distribution. Therefore, Spearman's rank correlation is utilized in this study.

The correlation coefficient values between the count differences and other indices are listed in Table 1 with the corresponding p values. The concurrent correlation values show only AMO, PDO, and SOCV are significantly (at 0.05 significance level) correlated with the count difference, and the correlation for AMO and PDO are only around 0.2 (absolute value). Since the count is a low-frequency signal, the impact from other climate phenomena may not be concurrent. As a result, we also calculate the correlation with time lags [CWD(t) vs Index(t + lag)] and identify the largest correlation with a specific lag. Those maximum correlation values and the associated time lags in years are also shown in Table 1. Except for SOI, all other indices demonstrate significant correlations at various lags. The initial maximum time lag is set at 15 years since the count is calculated in durations with 15 years as its half-length. If that maximum lag is increased to 20, the only change to the maximum correlation is that of the NAO from 0.13 to −0.19 with lag changes from lag −3 to lag −20.

The correlation results can also be demonstrated via the time series plots. Figure 4a displays CWD and SOCV values with the annual average values of other climate indices. To make the values in a similar range, the CWD values are normalized by taking zero mean and scaling by 3 times the standard deviation. Except for the original annual-based values of CWD and SOCV, oscillations with decadal or multidecadal scales are dominant. However, the oscillations of relatively high frequencies make it very difficult to see the relationships among those time series. To have a clearer picture of the impacts of the climate indices on the count difference, a moving average with the same time interval, 31 years as for CWD, is utilized. The results with a moving average are displayed in Figure 4b, and one can see the simple correlation relationship much easier with the smoothed data than with the original annual values. For example, the trend of PDO (green line) is coincident with the trend of CWD since around 1950. This coincidence cannot be identified with the unsmoothed data. After smoothing, lag −1 results in the highest correlation. The negative 1-yr lag means that we should shift the PDO right by 1 year to make the two time series coincident. The curves after 1950 in

Table 1. Correlation values between CWD and climate indices. The second and third columns are values of concurrent correlation coefficient (cc) and the corresponding *p* values. The fourth and fifth columns are for the maximum cc values among all lags with the Maxlag limit and the corresponding *p* values. The last column is the year shift of the climate indices for achieving the maximum cc.

Index	cc	*p* value	Max cc	*p* value	Lag
			Original data: Maxlag = 15		
AMO	-2.0×10^{-1}	3.0×10^{-2}	-2.7×10^{-1}	2.8×10^{-3}	−6
NAO	1.1×10^{-1}	2.4×10^{-1}	1.3×10^{-1}	1.4×10^{-1}	−3
PDO	2.1×10^{-1}	3.3×10^{-2}	$3.4 \times 10^{-1}01$	3.0×10^{-4}	7
SOI	-1.1×10^{-1}	2.3×10^{-1}	-1.6×10^{-1}	8.1×10^{-2}	−4
TPI	1.2×10^{-1}	1.9×10^{-1}	2.3×10^{-1}	1.1×10^{-2}	7
SOCV	4.3×10^{-1}	1.1×10^{-6}	7.5×10^{-1}	1.4×10^{-22}	−14
			Original data: Maxlag = 20		
AMO	-2.0×10^{-1}	3.0×10^{-2}	-2.7×10^{-1}	2.8×10^{-3}	−6
NAO	1.1×10^{-1}	2.4×10^{-1}	-1.9×10^{-1}	4.0×10^{-2}	−20
PDO	2.1×10^{-1}	3.3×10^{-2}	3.4×10^{-1}	3.0×10^{-4}	7
SOI	-1.1×10^{-1}	2.3×10^{-1}	-1.6×10^{-1}	8.1×10^{-2}	−4
TPI	1.2×10^{-1}	1.9×10^{-1}	2.3×10^{-1}	1.1×10^{-2}	7
SOCV	4.3×10^{-1}	1.1×10^{-6}	7.5×10^{-1}	1.4×10^{-22}	−14
			With MA: Maxlag = 15		
AMO	-2.5×10^{-1}	5.3×10^{-3}	-2.7×10^{-1}	2.7×10^{-3}	−5
NAO	1.7×10^{-1}	5.7×10^{-2}	4.4×10^{-1}	2.9×10^{-6}	15
PDO	4.6×10^{-1}	8.6×10^{-6}	4.7×10^{-1}	8.3×10^{-6}	−1
SOI	-5.3×10^{-1}	4.3×10^{-10}	-5.8×10^{-1}	6.2×10^{-12}	−2
TPI	3.7×10^{-1}	4.5×10^{-5}	5.4×10^{-1}	2.6×10^{-10}	15
SOCV	5.1×10^{-1}	2.2×10^{-9}	8.0×10^{-1}	2.0×10^{-27}	−15
			With MA: Maxlag = 20		
AMO	-2.5×10^{-1}	5.3×10^{-3}	-2.7×10^{-1}	2.7×10^{-3}	−5
NAO	1.7×10^{-1}	5.7×10^{-2}	4.8×10^{-1}	4.0×10^{-7}	20
PDO	4.6×10^{-1}	8.6×10^{-6}	4.7×10^{-1}	8.3×10^{-6}	−1
SOI	-5.3×10^{-1}	4.3×10^{-10}	-5.8×10^{-1}	6.2×10^{-12}	−2
TPI	3.7×10^{-1}	4.5×10^{-5}	5.6×10^{-1}	2.5×10^{-11}	18
SOCV	5.1×10^{-1}	2.2×10^{-9}	8.3×10^{-1}	1.8×10^{-30}	−18

Figure 4b clearly demonstrate this effect. In this case, the highest correlation between CWD and PDO is 0.47, higher than the 0.34 achieved without smoothing at lag 7 (Table 1).

The correlation improving with smoothed data is not a surprise. All correlation coefficients with the moving average values are higher (in absolute values) than those with the original annual values because the smoothing effects filter out the high-frequency oscillations and introduce/enhance autocorrelation. It is interesting to note that SOI results in higher correlation than SOCV after smoothing. However, the maximum correlations with optimal lags show that a leading SOCV with −18 lag leads to the highest correlation, as high as 0.83, among all indices. The correlation strength with SOI increases less than that for SOCV from 0.53 (negative) to 0.58 (negative) with lag −2. Nevertheless, the correlation with SOI is possibly an artifact. Before the smoothing, the SOI oscillates around zero with relatively high frequencies, and the amplitude is large. The smoothed SOI is of small amplitude in the oscillation

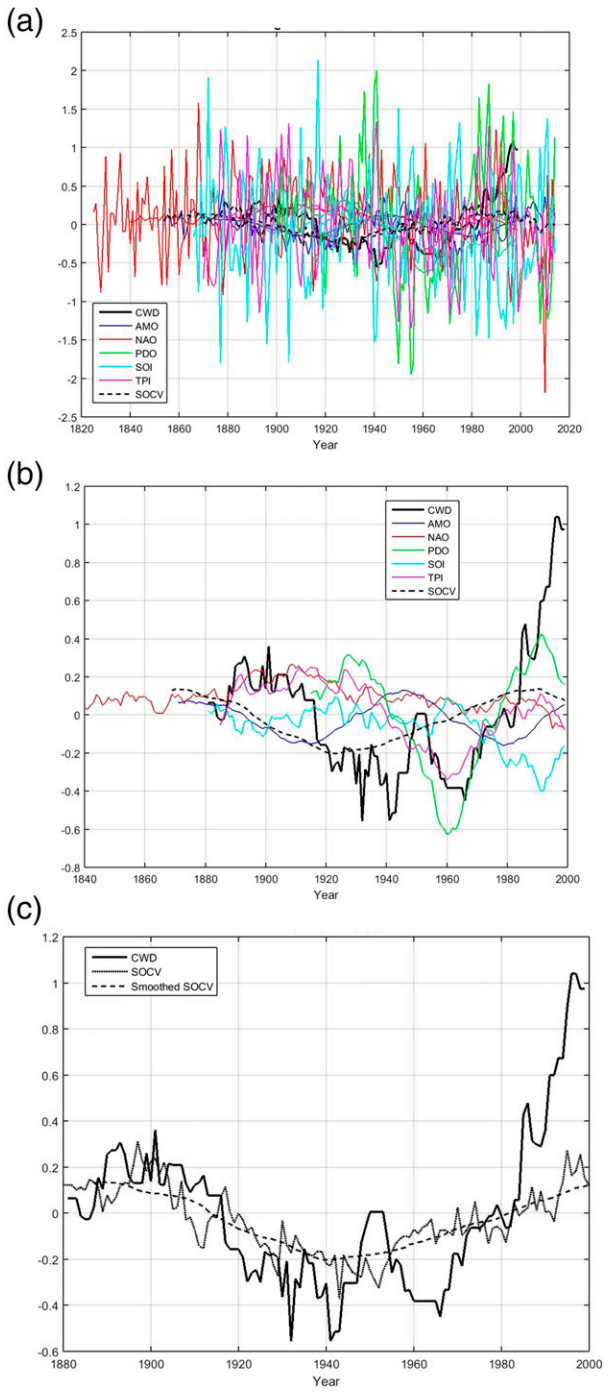

Figure 4. Time series of normalized CWD (with three std dev) and other climate indices. (a) Indices with original temporal annual resolution. (b) Smoothed index values with 31-yr moving average. (c) CWD and SOCV only. Both original annual SOCV and the smoothed SOCV are included. The SOCV are shifted right 18 years in (c).

except for the most recent 30 years and is of relatively high frequency. So, the high correlation is mainly due to the small-amplitude oscillations in the smoothed SOI, which does not make much sense. In contrast, the variability of the smoothed PDO is more prominent because of its high amplitude and low frequency, illustrating similar variability compared with CWD. Nevertheless, the amplitude modulation of SOI does increase and is consistent with the large ENSO impact in most recent years (Li et al. 2011; Burn and Palmer 2015).

With that said, the most interesting correlation result is that with SOCV, which not only gives the highest value but also demonstrates consistency with the lag. With the original annual SOCV values, the correlation is 0.43, which is much higher than the correlation with all other climate indices. After smoothing, the correlation is increased to 0.51, which is not much gain because the original SOCV is mainly for low-frequency variability, and it is much smoother than other climate indices. In searching for the optimal lag with the original data, the maximum correlation is 0.75 with a −14 lag. Similarly, the largest correlation detected from the smoothed data is 0.80 at −15 lag when the maximum lag is limited to 15. Since the lag is on the preset limit, the maximum lag is extended to 20, and the optimal lag is pinpointed at −18, at which the correlation is 0.83. If we use the concept of coefficient of determination R^2, we can say that SOCV can explain 69% change in CWD with an 18-yr lag. More importantly, the negative lag means that SOCV leads the CWD, and the change of SOCV can be used for the prediction of CWD and therefore the TC activity in the Atlantic. To see the lag impact, the SOCV is shifted by 18 years to the right and the result is displayed in Figure 4c. This figure exhibits strong consistent variability between CWD and SOCV.

Climate model simulations suggest the SOCV is generated in the Southern Ocean. Its mechanism is distinct from other longer time-scale variability, such as AMO. Park and Latif (2008) argue that the multidecadal variability in the Atlantic sector is generated in the North Atlantic, while the SOCV is driven in the Southern Ocean where sea ice change is considerably involved. Martin et al. (2013) further show that building up of heat in the middepth and its release to the atmosphere is a key to generate the SOCV. The source of heat is inflow of the North Atlantic Deep Water (NADW), which indicates a large-scale link between the Northern and Southern Hemispheres. The SOCV signal generated in the South Atlantic also propagates to the North Atlantic via different processes. Swingedouw et al. (2009) proposed three ways of connections: deep-water adjustment via oceanic waves, salinity anomaly advection, and wind impact on the NADW cell. Each has different response time scales in the model, of which the precise time scale may differ in the observation.

The physical link between the SOCV and TCs may be explained with one or a combination of these propagation dynamics. One strong candidate is the advective process, as illustrated by climate models (Vellinga and Wu 2004; Menary et al. 2012). In the advective processes, a strengthened NADW cell, or Atlantic meridional overturning circulation (MOC), linked to the SOCV, transports more heat to the Northern Hemisphere from the Southern Hemisphere and increases SST over the tropical and subtropical Atlantic, where development of TCs is active.

It must be pointed out that the correlation analysis above really shows that the variation in CWD is of long time scale, and its correlation with commonly used climate indices is weak. The correlation with SOCV is the only one showing a

strong relationship. Because any two time series of similar periods would result in high-correlation values because of the strong autocorrelation, the impact of the autocorrelation on the significance of the correlation is estimated. We used the widely accepted correction formula (Bretherton et al. 1999; McCarthy et al. 2015)

$$n_{\text{eff}} = n\frac{1 - a_1 a_2}{1 + a_1 a_2},$$

where n is the number of observations of time series and a_1 and a_2 are the lag-1 autocorrelation of each of the two time series, respectively, and find that the effective size of the data n_{eff} for the correlation between CWD and SOCV is reduced from 119 to 9.25. Nevertheless, the lagged correlation is so strong that even after the correction, the p value is still less than 0.05.

4. Conclusions and discussion

This work demonstrates how a centennial cycle of ENSO impacts the Atlantic TC activity and how this century-scale variation can be plausibly linked to the SOCV. To the best knowledge of the authors, this is the first study to reveal TC-related variation in centennial scale with nonproxy data, although this variation is not directly on TC activities. This work sheds light on two aspects of long-term TC prediction. One of them is on seasonal prediction. Right now, there are many efforts focused on seasonal predictions for the Atlantic hurricane activities, such as those by Colorado State University, the NOAA CPC, and the private British forecasting firm Tropical Storm Risk (http://www.tropicalstormrisk.com/forecasts.html). Among them, ENSO is an important predictor. The work showed above clearly reveals that the ENSO impact on the Atlantic TC activity is complicated, and the ENSO factor in the seasonal prediction should be modulated. An example of such work is the conditional ENSO impact on seasonal Atlantic TC prediction by Davis et al. (2015) in which the ENSO contribution is conditioned by AMO. This work suggests long-term variation such as SOCV could be used for the condition.

Another motivation for this work is for enhancing longer than seasonal TC prediction. Multiyear TC prediction should be more useful for insurance purposes and long-term disaster mitigation. Similar topics are investigated in several studies (e.g., Vecchi et al. 2013; Smith et al. 2010). Vecchi et al. (2013) investigated the multiyear prediction of TC frequency in the North Atlantic with climate models for SSTs and a statistical emulator for TC frequency, which is a function of some aggregated SSTs (Vecchi et al. 2011). As in other studies on long-term TC activity changes, the majority of the work is based on outputs from climate models, and the focus is on long-term climate changes as well as the associated changes in the Atlantic TC activities (e.g., Dunstone et al. 2011; Dunstone et al. 2013: Caron et al. 2014; Caron et al. 2015). This study and the corresponding SOCV data could be used for even longer-term forecasting of the Atlantic TC activity.

Acknowledgments. We thank one of anonymous reviewers for pointing out the data distribution issue, which leads to the change from Pearson's r to Spearman's rank correlation analysis. Publication of this article was funded in part by the George Mason University Libraries Open Access Publishing Fund.

References

Bell, G. D., and M. Chelliah, 2006: Leading tropical modes associated with interannual and multidecadal fluctuations in North Atlantic hurricane activity. *J. Climate*, **19**, 590–612, https://doi.org/10.1175/JCLI3659.1.

Biondi, F., A. Gershunov, and D. R. Cayan, 2001: North Pacific decadal climate variability since 1661. *J. Climate*, **14**, 5–10, https://doi.org/10.1175/1520-0442(2001)014<0005:NPDCVS>2.0.CO;2.

Bretherton, C. S., M. Widmann, V. P. Dymnikov, J. M. Wallace, and I. Blade, 1999: The effective number of spatial degrees of freedom of a time-varying field. *J. Climate*, **12**, 1990–2009, https://doi.org/10.1175/1520-0442(1999)012<1990:TENOSD>2.0.CO;2.

Burn, M. J., and S. E. Palmer, 2015: Atlantic hurricane activity during the last millennium. *Sci. Rep.*, **5**, 12838, https://doi.org/10.1038/srep12838.

Caron, L.-P., C. G. Jones, and F. Doblas-Reyes, 2014: Multi-year prediction skill of Atlantic hurricane activity in CMIP5 decadal hindcasts. *Climate Dyn.*, **42**, 2675–2690, https://doi.org/10.1007/s00382-013-1773-1.

——, L. Hermanson, and F. J. Doblas-Reyes, 2015: Multiannual forecasts of Atlantic U.S. tropical cyclone wind damage potential. *Geophys. Res. Lett.*, **42**, 2417–2425, https://doi.org/10.1002/2015GL063303.

Cobb, K. M., N. Westphal, H. R. Sayani, J. T. Watson, E. D. Lorenzo, H. Cheng, R. L. Edwards, and C. D. Charles, 2013: Highly variable El Niño–Southern Oscillation throughout the Holocene. *Science*, **339**, 67–70, https://doi.org/10.1126/science.1228246.

CPC, 2015: Cold and warm episodes by season. Accessed 28 December 2015, http://www.cpc.ncep.noaa.gov/products/analysis_monitoring/ensostuff/ensoyears.shtml.

Davis, K., X. Zeng, and E. A. Ritchie, 2015: A new statistical model for predicting seasonal North Atlantic hurricane activity. *Wea. Forecasting*, **30**, 730–741, https://doi.org/10.1175/WAF-D-14-00156.1.

Dunstone, N. J., D. M. Smith, and R. Eade, 2011: Multi-year predictability of the tropical Atlantic atmosphere driven by the high latitude North Atlantic Ocean. *Geophys. Res. Lett.*, **38**, L14701, https://doi.org/10.1029/2011GL047949.

——, ——, B. B. B. Booth, L. Hermanson, and R. Eade, 2013: Anthropogenic aerosol forcing of Atlantic tropical storms. *Nat. Geosci.*, **6**, 534–539, https://doi.org/10.1038/ngeo1854.

Emanuel, K., 2005: Increasing destructiveness of tropical cyclones over the past 30 years. *Nature*, **436**, 686–688, https://doi.org/10.1038/nature03906.

Enfield, D. B., A. M. Mestas-Nunez, and P. J. Trimble, 2001: The Atlantic multidecadal oscillation and its relation to rainfall and river flows in the continental U.S. *Geophys. Res. Lett.*, **28**, 2077–2080, https://doi.org/10.1029/2000GL012745.

ESRL, 2015: Southern Oscillation index (SOI). Accessed 28 December 2015, http://www.esrl.noaa.gov/psd/gcos_wgsp/Timeseries/Data/soi.long.data.

——, 2017: Climate indices: Monthly atmospheric and ocean time series. Accessed 5 July 2017, https://www.esrl.noaa.gov/psd/data/climateindices/list/.

Goldenberg, S. B., C. W. Landsea, A. M. Mestas-Nunez, and W. M. Gray, 2001: The recent increase in Atlantic hurricane activity: Causes and implications. *Science*, **293**, 474–479, https://doi.org/10.1126/science.1060040.

Gray, W. M., 1984: Atlantic seasonal hurricane frequency. Part I: El Niño and 30 mb quasi-biennial oscillation influences. *Mon. Wea. Rev.*, **112**, 1649–1668, https://doi.org/10.1175/1520-0493(1984)112<1649:ASHFPI>2.0.CO;2.

Hanley, D. E., M. A. Bourassa, J. J. O'Brien, S. R. Smith, and E. R. Spade, 2003: A quantitative evaluation of ENSO indices. *J. Climate*, **16**, 1249–1258, https://doi.org/10.1175/1520-0442(2003)16<1249:AQEOEI>2.0.CO;2.

Henley, B. J., J. Gergis, D. J. Karoly, S. B. Power, J. Kennedy, and C. K. Folland, 2015: A tripole index for the interdecadal Pacific oscillation. *Climate Dyn.*, **45**, 3077–3090, https://doi.org/10.1007/s00382-015-2525-1.

HRD, 2015: Frequently asked questions. Accessed 28 December 2015, http://www.aoml.noaa.gov/hrd/tcfaq/E11.html.

Hurrell, J. W., 1995: Decadal trends in the North Atlantic Oscillation and relationships to regional temperature and precipitation. *Science*, **269**, 676–679, https://doi.org/10.1126/science.269.5224.676.

Jones, P. D., T. Jonsson, and D. Wheeler, 1997: Extension to the North Atlantic Oscillation using early instrumental pressure observations from Gibraltar and south-west Iceland. *Int. J. Climatol.*, **17**, 1433–1450, https://doi.org/10.1002/(SICI)1097-0088(19971115)17:13<1433::AID-JOC203>3.0.CO;2-P.

Klotzbach, P. J., 2007: Revised prediction of seasonal Atlantic basin tropical cyclone activity from 1 August. *Wea. Forecasting*, **22**, 937–949, https://doi.org/10.1175/WAF1045.1.

——, 2011: A simplified Atlantic basin seasonal hurricane prediction scheme from 1 August. *Geophys. Res. Lett.*, **38**, L16710, https://doi.org/10.1029/2011GL048603.

Landsea, C. W., and J. L. Franklin, 2013: Atlantic hurricane database uncertainty and presentation of a new database format. *Mon. Wea. Rev.*, **141**, 3576–3592, https://doi.org/10.1175/MWR-D-12-00254.1.

——, G. A. Vecchi, L. Bengtsson, and T. R. Knutson, 2010: Impact of duration thresholds on Atlantic tropical cyclone counts. *J. Climate*, **23**, 2508–2519, https://doi.org/10.1175/2009JCLI3034.1.

Latif, M., T. Martin, and W. Park, 2013: Southern Ocean sector centennial climate variability and recent decadal trends. *J. Climate*, **26**, 7767–7782, https://doi.org/10.1175/JCLI-D-12-00281.1.

Li, J., S.-P. Xie, E. R. Cook, G. Huang, R. D'Arrigo, F. Liu, J. Ma, and X.-T. Zheng, 2011: Interdecadal modulation of El Niño amplitude during the past millennium. *Nat. Climate Change*, **1**, 114–118, https://doi.org/10.1038/nclimate1086.

Mann, M. E., J. D. Woodruff, J. P. Donnelly, and Z. Zhang, 2009: Atlantic hurricanes and climate over the past 1,500 years. *Nature*, **460**, 880–883, https://doi.org/10.1038/nature08219.

Martin, T., W. Park, and M. Latif, 2013: Multi-centennial variability controlled by Southern Ocean convection in the Kiel Climate Model. *Climate Dyn.*, **40**, 2005–2022, https://doi.org/10.1007/s00382-012-1586-7.

McCarthy, G. D., I. D. Haigh, J. J. Hirschi, J. P. Grist, and D. A. Smeed, 2015: Ocean impact on decadal Atlantic climate variability revealed by sea-level observations. *Nature*, **521**, 508–510, https://doi.org/10.1038/nature14491.

Menary, M. B., W. Park, K. Lohmann, M. Vellinga, M. D. Palmer, M. Latif, and J. H. Jungclaus, 2012: A multimodel comparison of centennial Atlantic meridional overturning circulation variability. *Climate Dyn.*, **38**, 2377–2388, https://doi.org/10.1007/s00382-011-1172-4.

Minobe, S., 1997: A 50–70 year climatic oscillation over the North Pacific and North America. *Geophys. Res. Lett.*, **24**, 683–686, https://doi.org/10.1029/97GL00504.

Park, W., and M. Latif, 2008: Multidecadal and multicentennial variability of the meridional overturning circulation. *Geophys. Res. Lett.*, **35**, L22703, https://doi.org/10.1029/2008GL035779.

Patricola, C. M., P. Chang, and R. Saravanan, 2015: Degree of simulated suppression of Atlantic tropical cyclones modulated by flavour of El Niño. *Nat. Geosci.*, **9**, 155–160, https://doi.org/10.1038/ngeo2624.

Philander, S. G., 1990: *El Niño, La Niña, and the Southern Oscillation.* Academic Press, 293 pp.

Smith, D. M., R. Eade, N. Dunstone, D. Fereday, J. M. Murphy, H. Pohlmann, and A. Scaife, 2010: Skillful multi-year predictions of Atlantic hurricane frequency. *Nat. Geosci.*, **3**, 846–849, https://doi.org/10.1038/ngeo1004.

Stevenson, S., 2012: Significant changes to ENSO strength and impacts in the twenty-first century: Results from CMIP5. *Geophys. Res. Lett.*, **39**, L17703, https://doi.org/10.1029/2012GL052759.

Swingedouw, D., T. Fichefet, H. Goosse, and M. F. Loutre, 2009: Impact of transient freshwater releases in the Southern Ocean on the AMOC and climate. *Climate Dyn.*, **33**, 365–381, https://doi.org/10.1007/s00382-008-0496-1.

Vecchi, G. A., M. Zhao, H. Wang, G. Villarini, A. Rosati, A. Kumar, I. M. Held, and R. Gudgel, 2011: Statistical–dynamical predictions of seasonal North Atlantic hurricane activity. *Mon. Wea. Rev.*, **139**, 1070–1082, https://doi.org/10.1175/2010MWR3499.1.

——, and Coauthors, 2013: Multiyear predictions of North Atlantic hurricane frequency: Promise and limitations. *J. Climate*, **26**, 5337–5357, https://doi.org/10.1175/JCLI-D-12-00464.1.

Vellinga, M., and P. L. Wu, 2004: Low-latitude freshwater influence on centennial variability of the Atlantic thermohaline circulation. *J. Climate*, **17**, 4498–4511, https://doi.org/10.1175/3219.1.

Webster, P., G. Holland, J. Curry, and H. Chang, 2005: Changes in tropical cyclone number, duration, and intensity in a warming environment. *Science*, **309**, 1844–1846, https://doi.org/10.1126/science.1116448.

Zhang, Y., J. M. Wallace, and D. S. Battisti, 1997: ENSO-like interdecadal variability: 1900–93. *J. Climate*, **10**, 1004–1020, https://doi.org/10.1175/1520-0442(1997)010<1004:ELIV>2.0.CO;2.